2-1-2015

# Load transfer at the distal ulna following simulated distal radius fracture malalignment.

Louis M Ferreira

Gillian S Greeley

James A Johnson

Graham J W King

# Load Transfer at the Distal Ulna Following Simulated Distal Radius Fracture Malalignment

Louis M. Ferreira, PhD, Gillian S. Greeley, PhD, James A. Johnson, PhD, Graham J. W. King, MD, MSc

**Purpose** To measure the effects of distal radius malalignment on loading at the distal ulna.

**Methods** Using an adjustable mechanism to simulate angulated and translated malalignments, clinically relevant distal radius deformities were simulated in a cadaveric model. A custom-built load cell was inserted just proximal to the native ulna head to measure the resultant force and torque in the distal ulna. Loads were measured before and after transecting the triangular fibrocartilage complex (TFCC).

**Results** There was an increase in distal ulna load and torque with increasing dorsal translation and angulation. Combined conditions of angulation and translation increased force and torque in the distal ulna to a greater extent than with either condition in isolation. Transecting the TFCC resulted in a reduction in distal ulna load and torque.

**Conclusions** A progressive increase in load at the distal ulna was observed with increasing severity of malalignment, which may be an important contributor to residual ulnar wrist pain and dysfunction. However, no clear-cut threshold of malalignment of a dorsally angulated and translated distal radius fracture was identified. These observations suggest that radius deformities cause articular incongruity, which increases TFCC tension and distal radioulnar joint load. Cutting of the TFCC decreased distal ulna loading, likely by releasing the articular constraining effect of the TFCC on the distal radioulnar joint, allowing the radius to rotate more freely with respect to the ulna.

**Clinical relevance** Anatomical reduction of a distal radius fracture minimizes the forces in the distal ulna and may reduce residual ulnar wrist pain and dysfunction. *(J Hand Surg Am. 2015;40(2):217–223. Copyright © 2015 by the American Society for Surgery of the Hand. All rights reserved.)*

**Key words** DRUJ, distal radius, distal ulna, fracture malalignment, joint loads.

*From the Bioengineering Research Laboratory, Roth|McFarlane Hand and Upper Limb Centre, Lawson Health Research Institute, St. Joseph's Health Care London; and the Department of Mechanical & Materials Engineering, the Department of Biomedical Engineering, the Department of Surgery, and the Department of Medical Biophysics, Western University, London, Ontario, Canada.*

Received for publication June 11, 2014; accepted in revised form October 7, 2014.

Dr. Yves Bureau provided statistical advice. Brendon Beaton codesigned the load cell and cowrote the calibration software.

No benefits in any form have been received or will be received related directly or indirectly to the subject of this article.

**Corresponding author:** Graham J. W. King, MD, MSc, Roth|McFarlane Hand and Upper Limb Centre, St. Joseph's Health Centre, 268 Grosvenor St., London, Ontario, Canada, N6A 4L6; e-mail: gking@uwo.ca.

0363-5023/15/4002-0002$36.00/0
http://dx.doi.org/10.1016/j.jhsa.2014.10.012

DISTAL RADIUS FRACTURES COMPRISE one-sixth of all fractures,[1–6] with a cumulative lifetime incidence of 15% for women and 3% for men.[7,8] Displaced fractures have a tendency to redisplace with cast immobilization, commonly resulting in residual deformities.[9] Radial shortening and dorsal angulation are associated with a high incidence of residual ulnar wrist pain, weakness and stiffness.[10–16] Corrective osteotomies frequently do not restore normal osseous alignment or function,[16] and more than 50% will exhibit posttraumatic arthritis.[17] With improved methods of fixation and computer-assisted surgery,[18,19] anatomical positioning and healing of distal radius fractures is possible; however, the magnitude and

pattern of displacement where surgical treatment is indicated are not yet defined.[10]

A variety of studies have examined the kinematic effects of a malunion after Colles fractures,[10,20–22] and 1 quantified the effect of malalignment on joint loads.[23] This *in vitro* biomechanical study by Hirahara et al[23] examined the effects of dorsally angulated fractures and found that resistance torque during forearm rotation increased with increasing degrees of distal radius malalignment. Another study quantified the magnitude of the distal radioulnar joint (DRUJ) reaction force throughout motion using an instrumented ulna head implant capable of measuring load transfer across the DRUJ, finding that the primary influence on joint load was related to the position of the ulna within the sigmoid notch of the radius, a function of the forearm position in rotation.[24]

Our objective was to measure the effects of distal radius malalignment and dividing triangular fibrocartilage complex (TFCC) on loading at the distal ulna. Using an adjustable mechanism previously designed and detailed by Fraser and coworkers,[25] we simulated clinically relevant distal radius deformities in a cadaveric model. A custom-built load cell was inserted just proximal to the native ulna head to measure the distal ulna load. We hypothesized that distal radius malalignment increases loading at the distal ulna and that ulna loads are lowest with the simulated distal radius fragment in its native position.

## MATERIALS AND METHODS

### Design of an instrumented implant

A load cell capable of measuring medial-lateral (ML) force, anterior-posterior (AP) force and inferior-superior (IS) axis torque was developed. To position the load cell in the distal ulna, an implant was designed with a distal component stem, a proximal component stem, a removable spacer, and the load cell (Fig. 1). The implant has both a spacer for specimen preparation and the instrumented load cell for testing. The spacer and load cell were designed similarly except that the spacer has a slightly smaller diameter (6 mm) than the instrumented load cell (8 mm). The smaller diameter facilitated maintaining an intact bone bridge during the insertion and cementing process.

The distal component was designed with a rectangular, notched stem for cementing into the head of the ulna, and the opposite end accepts the spacer and load cell. Similarly, the proximal component includes a square, notched end, and the reverse end has provisions to accept the proximal end of the spacer or load cell. The stem diameter was chosen to be an appropriate size to fit even the smallest specimens while allowing for an adequate cement mantle, and the notching assists with fixation. Figure 1 shows the ulna implant *in situ*, with the adjustable mechanism that simulates malalignment deformities of dorsal angulation and dorsal translation.

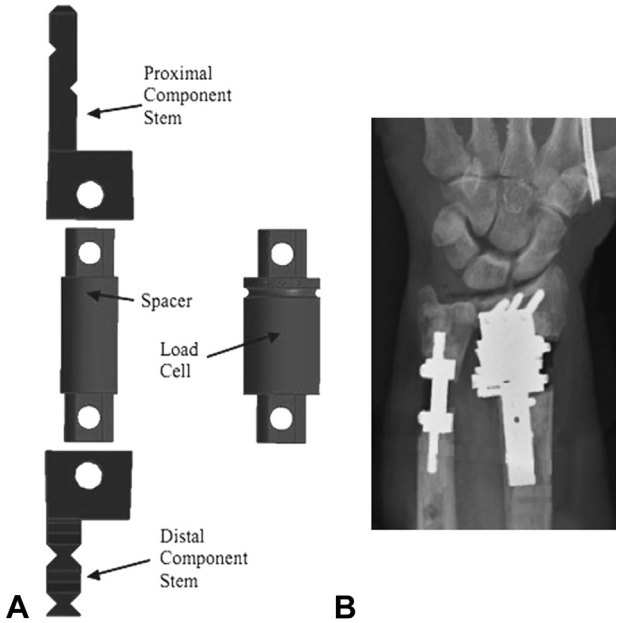


**FIGURE 1:** Distal ulna load cell system. **A** An exploded view of the instrumented distal ulna load cell. This implantable system comprises 4 parts: the distal component stem, the proximal component stem, the spacer, and the load cell. For surgical setup, a spacer was used (left); however, for testing purposes, this was removed and replaced with the instrumented load cell (right). **B** The distal implant system is shown *in situ*. Also visible is the distal radius malalignment implant.

To quantify load, 4 shear-sensitive rosette strain gauges (Model #062TV, Vishay Intertechnology Inc., Malvern, PA) were placed at 90° from one another around the circumference of the load cell. Each rosette gauge was made up of 2 strain elements, which were wired into independent quarter bridges. These 8 quarter bridges were combined into 6 axis-dependent strain values and the load cell was calibrated with a custom-designed appliance according to the Berme Calibration Technique.[26] From this, the clinically relevant AP force, ML force, and IS torque were quantified.

### Specimen preparation and surgical procedures

Eight fresh frozen upper extremities (mean age, 71 y; range, 49–84 y; 6 male, 4 right) were used. All were radiographed before testing to exclude specimens with arthritis or previous fracture. The specimens

were amputated through the midhumerus, and prepared for testing using a forearm motion simulator (Fig. 2), which has been previously described.[27,28] The distal radius was exposed through a volar approach. An osteotomy was performed just proximal to the sigmoid notch and the 3-degree of freedom modular implant designed to simulate distal radius deformities was secured to the distal radius.[25] This allowed for accurate adjustment of dorsal angulation and translation. Anatomical alignment of the distal radius was maintained by a bone bridge technique previously described by Fraser et al[25] using the same adjustable instrumented implant.

The distal ulna was approached through a longitudinal incision on the subcutaneous border, just proximal to the ulna head. The interval between the extensor and the flexor carpi ulnaris tendons was developed to expose the ulna. Using a microsagittal saw, a 16-mm volar segment of the ulna was removed approximately 1.5 cm proximal to the ulna head to accommodate insertion of the load cell while preserving a bone bridge on the dorsal side of the ulna. This ensured that the alignment of the native head with respect to the proximal ulna was maintained both during and after load cell insertion. The medullary canal and ulna head were reamed and polymethylmethracrylate was injected into the canals. The ulna load cell was separated, the distal stem was inserted into the ulna head cavity, and the proximal stem was inserted into the medullary canal. Once in position, the spacer was reattached to the proximal and distal ends to maintain the implant's default configuration, and the construct was held firmly in position until the cement had cured. The ulna bone bridge was then divided.

The specimen was mounted in a forearm motion simulator (Fig. 2). Two servo motors were used to actuate the prime movers (ie, agonist and antagonist) of forearm rotation (ie, biceps and pronator teres). Linear pneumatic actuators were used for muscle loads to triceps, wrist flexors/extensors, and pronator quadratus. In-line load cells were used to monitor and control loads to the biceps and pronator teres as per Gordon et al.[29] An electromagnetic tracker (Flock of Birds, Ascension Technologies Corp, Shelburne, VT) was used for closed-loop control of forearm rotation, by rigidly mounting a receiver to the radius and ulna.

The load cell spacer was removed and the instrumented load cell was installed. The incisions were repaired and the specimens were kept moist using saline irrigation of the soft tissues as well as by repeated closure of the skin following each implant adjustment.

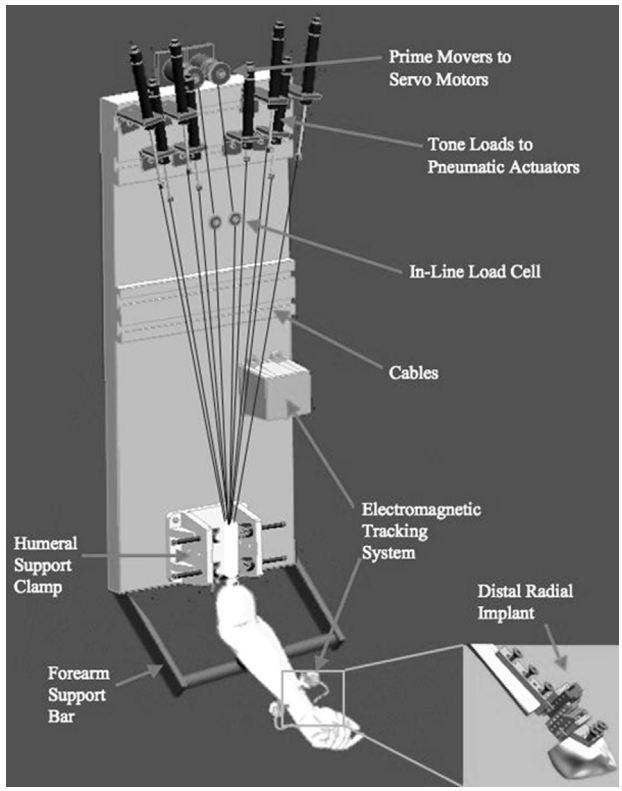


**FIGURE 2:** Motion-controlled upper limb testing system. Two servo motors were used to actuate the prime movers (ie, agonist and antagonist) of forearm rotation (ie, biceps and pronator teres). Linear pneumatic actuators were used for muscle loads to triceps, wrist flexors/extensors, and pronator quadratus. The in-line load cells were used to monitor and control loads to the biceps and pronator teres. An electromagnetic tracker was used for closed-loop control of forearm rotation. Inset: Device to simulate angular and translation malalignments of the distal radius.

During motion control, the relative muscle loading ratios for the pronator agonists (pronator teres and pronator quadratus) were maintained at 56% and 44%, respectively, and for the supinator agonists (biceps brachii and supinator) were 67% and 33%, respectively.[29] Muscle load magnitudes were automatically adjusted through the feedback loop with the apportioning approach. The tendon forces required to simulate active supination and pronation across all conditions of malalignment were quantified.

### Testing procedure

Active pronation and supination motions were simulated in each specimen while the elbow was flexed at 90°, and kinematic data were recorded in this intact configuration. The electromagnetic tracking system quantified the position of the radius relative to the ulna.

This study consisted of 2 phases to examine the effects before and after simulated soft tissue

**TABLE 1. Ulna Load and Torque (± 1 SD) Across Forearm Rotation With the Distal Radius in the Native Position**

| | Force (N) | | |
|---|---|---|---|
| | Pronated | Neutral | Supinated |
| Pronation trial | 6.4 (5.6) | 6.5 (7.1) | 9.0 (10.6) |
| Supination trial | 5.9 (5.8) | 6.1 (6.0) | 8.2 (10.3) |
| | **Torque (Nmm)** | | |
| | Pronated | Neutral | Supinated |
| Pronation trial | −40.0 (25.1) | −50.0 (38.0) | −66.3 (50.7) |
| Supination trial | −40.4 (31.3) | −50.8 (39.9) | −68.3 (59.1) |

Notes: Loading at the distal ulna was found to range between 5 and 9 N. Supinated data are at 45° of supination and pronated are at 30° of pronation. There was greater distal ulna load and torque with the forearm in supination relative to pronation ($P = .01$; $P = .01$). The ulna torque decreased following TFCC sectioning ($P = .03$), but not the ulna load.

disruption of the DRUJ. All soft tissue stabilizers of the DRUJ were intact in the first phase of the study while the effects of simulated distal radius deformities were evaluated. The instrumented implant was used to simulate dorsally angulated and translated distal radius deformities. Two factors were simulated: conditions of 0°, 10°, 20°, and 30° of dorsal angulation from the original palmar tilt, and conditions of 0, 5, and 10 mm of dorsal translation. Each of these dorsal angulation and translation factors were evaluated independently and in combination.

The testing protocol was repeated after dividing of the TFCC to examine the effects of a simulated ulnar-sided ligament injury on distal ulna loading, which commonly occurs in association with distal radius deformities. The TFCC was divided by detaching it from its attachment on the ulna using an open surgical approach. We confirmed a complete sectioning at the end of the testing protocol by disarticulating the wrist.

### Outcome variables and statistics

Following completion of testing, the joints were disarticulated and ulna surface landmarks were digitized in order to create a clinically relevant ulna reference frame. Calibrated load cell output was transformed to the ulna frame so that loads were expressed in anatomical directions. The forces in the AP and ML directions measured at the distal ulna were resolved into the resultant transverse distal ulna load, hereafter referred to as the (distal) ulna load. In addition, torque about the IS axis of the ulna was quantified.

Force and torque on the distal ulna were analyzed independently. In order to determine whether differences existed between pronation and supination motion trials for force and torque, 2-way repeated measures analyses of variance were conducted examining the factors of TFCC state and forearm motion. Four-way repeated measures analyses of variance were used to determine whether there were differences in force or torque (dependent variable) as a result of the factors of TFCC state, angulation, translation, and rotation (independent variables). Using the active simulation method, the range of rotation achieved commonly by all specimens was 90° for supination motion (45° pronated to 45° supinated) and 75° for pronation motion (45° supinated to 30° pronated). Statistical analysis was performed at 15° increments with significant set at *P less* than .05.

## RESULTS

Ulna load increased during forearm supination ($P = .01$) with the distal radius in the native position (Table 1); however, there was no effect from the direction of forearm rotation. Similarly, there was greater torque on the ulna when the forearm was in supination than in pronation ($P = .009$) (Table 1). Although the distal ulna load tended to decrease following sectioning of the TFCC, this was not statistically significant (Fig. 3). The decrease in torque observed with sectioning the TFCC was significant ($P = .03$) (Table 1).

Ulna load was greater with increasing dorsal translation ($P = .008$) and angulation ($P = .002$) of the simulated distal radius deformities (Fig. 3). This was most evident in terminal pronation and supination. Combined angulation and translation caused a greater ulna load than either of the conditions in isolation ($P = .002$). Dividing the TFCC resulted in a statistically

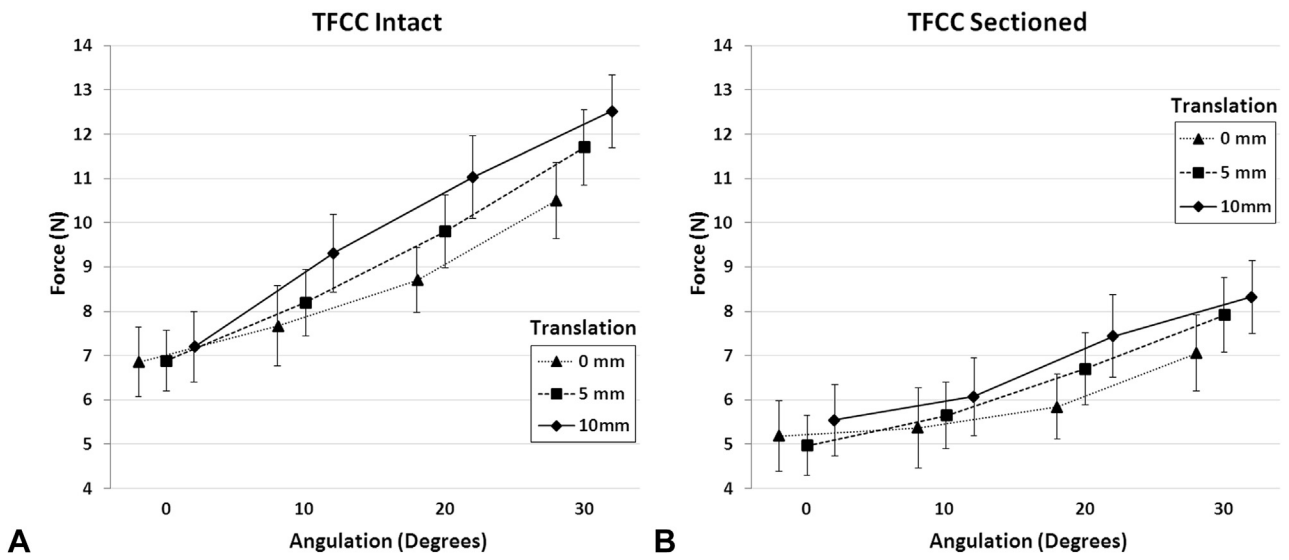


**FIGURE 3:** Distal radius malalignment and its effect on distal ulna load. The relationship between the deformity of the distal radius and the ulna load for intact **A** and sectioned **B** TFCC ligaments at neutral rotation. Increasing translation or angulation caused an increase in ulna load ($P = .008$ and $P = .002$, respectively). Combining these deformities had a greater effect than either in isolation ($P = .002$). Sectioning the TFCC trended toward decreased ulna load for all conditions, but not significantly. Maximum SD across all conditions was 8.8 N (intact) and 6.3 N (sectioned).

insignificant reduction in ulna load for all malalignment conditions.

There was an increase in torque with increasing dorsal translation ($P = .001$) and angulation ($P = .002$) (Table 1). There was greater torque when the forearm was in the supinated position than in the pronated position ($P = .005$), with no effect from the direction of forearm rotation. Similar to ulna load, when the angulation and translation conditions were combined, a larger torque was evident than with either of the conditions in isolation ($P = .03$). Sectioning the TFCC resulted in a reduction in ulna torque ($P = .02$).

## DISCUSSION

The results of this study support the concept of Adams[10] that displaced fractures and malunions of the radius alter the configuration of the TFCC causing increased tissue tension. Our findings agree with Hirahara et al,[23] showing that increasing dorsal angulation and translation result in a progressive increase of force and torque at the distal ulna. We also observed that combined radius angulation and translation resulted in greater ulna load and torque than isolated deformities. The additional tension in the TFCC increased loading at the distal ulna. The magnitude of distal ulna load in this study increased to 165% of the native load with the most extreme malalignment. We speculate that this increased loading at the distal ulna may be why patients commonly complain of pain in the setting of healed angulated and translated fractures of the distal radius.

There are a variety of biomechanical reasons for the increase in distal ulna load that occurs with larger magnitudes of distal radius malalignment. Radius shortening and dorsal translation, as a consequence of dorsal angulation in isolation, effectively increase the tension on the TFCC. Joint incongruity produced by dorsal angulation and dorsal translation causes an interosseous membrane tightness[22] and dorsal radioulnar ligament strain.[21] Distal radius malalignment increased the load by 165% of the native condition, and transecting the ligaments decreased the load to 60% of the native condition. These studies support our finding that the biomechanics of the DRUJ can be altered with relatively small changes in native osseous position and ligamentous integrity.

There was a 60% decrease in distal ulna load and a 35% decrease in torque after transecting the TFCC. Most investigators agree that the TFCC is the primary stabilizer of the distal radioulnar joint.[22,30,31] With the TFCC intact, 2 forces are registered at the load cell: DRUJ contact force and tension in the TFCC. When the TFCC is divided, this 1 component of force is removed, causing a decrease in the load at the distal ulna. With simulated distal radius malalignment, the relative position of the radius with respect to the ulna changes. This lengthens and strains the TFCC as exhibited by the increased loading observed at the distal ulna. Transecting the TFCC simulates ligament

rupture or a basal ulna styloid fracture such as commonly occurs clinically in patients with distal radius fractures. This releases the constraining effect of the TFCC on the DRUJ and causes a reduction in joint loading.

The overall performance of the instrumented distal ulna implant in this study was found to be acceptable. The interposed implant design allowed the use of the native ulna head, and the bone-bridge implantation technique ensured that the ulna head remained in its intact location. No loosening of the load cell was observed in any specimen during testing, and the forces and torque were within the load cell's design range.

Others have examined DRUJ loads using *in vitro* models. Shaaban et al[32] employed an externally applied axial load of 5 and 10 kg through the hand and found that DRUJ loading peaked at 6 N throughout forearm rotation for both levels of applied load. These authors used pressure-sensitive film inserted into the DRUJ to quantify load. Gordon et al[24] developed an instrumented ulna head implant to examine joint loading at the distal ulna. That study reported ulna load of 2 to 8 N but did not maintain the native ulna head, and so it may not be representative of the native condition. Despite differences in testing methodologies, the values reported in this study are in general agreement overall, because the magnitude of joint load through the distal ulna with the distal radius in the native position was found to range between 5.9 ± 5.8 N and 9.0 ± 10.6 N, and the torque values were between 40 ± 24 Nmm and 68 ± 59 Nmm, similar to other studies.[24,32]

The greatest ulna loads occurred when the forearm was fully supinated, which agrees with 2 previous studies.[24,32] Despite muscle loads were markedly different between pronation and supination, the direction of forearm rotation did not influence ulna loads. The absence of this influence was also found in a previous study, which also concluded that the primary factor in distal ulna loading was the position of the ulna head within the sigmoid notch.[24]

There are some limitations of this study. First, we performed all of our testing with the elbow at 90° of flexion. Previous studies have shown load-sharing at the wrist depends on the varus-valgus position of the elbow.[33–36] However, althoughwe did constrain the elbow at 90° of flexion, it was free to move in varus and valgus. Second, the net tension measured by the load cell included TFCC tension, and as such, we were unable to isolate the individual effects of TFCC tension and articular loading on the distal ulna. To measure loading directly at the DRUJ is challenging. Although pressure-sensitive films have been employed with some success in static applications (Rajaai SM, Walsh WR, Schindhelm K. Cadaver studies to obtain articular pressure in the distal radioulnar joint using Fuji prescale pressure sensitive film. *Engineering in Medicine and Biology Society, Proceedings of the 18th Annual International Conference of the IEEE*. 1996;489–490),[32,37] the invasiveness and challenges with placement and stability while testing preclude their use for a motion-based study. Third, this was an *in vitro* biomechanical study and the simulation of muscle loading to achieve forearm rotation may not have precisely replicated those loads that occur *in vivo*. Despite these limitations, our data do provide a valid tool for comparative measurements across the radius deformities assessed.

Our results improve understanding of the causes of pain with distal radius deformities and provide clearer indications for surgical treatment. This study advances previous research that examined single-plane distal radius malalignment and further elucidates the effects of complex deformities on distal ulna load and torque. Limited pronation and supination, which has been reported following distal radius deformities, may be caused by the lack of congruency at the DRUJ and increased tension in the TFCC; this work demonstrates how this is manifested by a progressive increase in force and torque in the distal ulna.

## REFERENCES


1. Souer JS, Lozano-Calderon SA, Ring D. Predictors of wrist function and health status after operative treatment of fractures of the distal radius. *J Hand Surg Am*. 2008;33(2):157–163.
2. Cooney WP. Fractures of the distal radius. A modern treatment-based classification. *Orthop Clin North Am*. 1993;24(2):211–216.
3. Maschke SD, Evans PJ, Schub D, Drake R, Lawton JN. Radiographic evaluation of dorsal screw penetration after volar fixed-angle plating of the distal radius: a cadaveric study. *Hand (N Y)*. 2007;2(3):144–150.
4. Lill CA, Goldhahn J, Albrecht A, Eckstein F, Gatzka C, Schneider E. Impact of bone density on distal radius fracture patterns and comparison between five different fracture classifications. *J Orthop Trauma*. 2003;17(4):271–278.
5. Belloti JC, Tamaoki MJ, Franciozi CE, et al. Are distal radius fracture classifications reproducible? Intra and interobserver agreement. *Sao Paulo Med J*. 2008;126(3):180–185.
6. Nesbitt KS, Failla JM, Les C. Assessment of instability factors in adult distal radius fractures. *J Hand Surg Am*. 2004;29(6):1128–1138.
7. Graf S. Fractures of the distal end of the distal radius: Classification of treatment and indications for external fixation. *Injury*. 1994;25:14–25.
8. Levine MA, ed. *Fractures of the Distal Radius. Orthop Knowl Update, Trauma*. Rosemont, IL: AAOS; 1996;67–82.
9. Mackenney PJ, McQueen MM, Elton R. Prediction of instability in distal radial fractures. *J Bone Joint Surg Am*. 2006;88(9):1944–1951.
10. Adams BD. Effects of radial deformity on distal radioulnar joint mechanics. *J Hand Surg Am*. 1993;18(3):492–498.
11. Fernandez DL. Correction of post-traumatic wrist deformity in adults by osteotomy, bone-grafting, and internal fixation. *J Bone Joint Surg Am*. 1982;64(8):1164–1178.

12. Fernandez DL. Radial osteotomy and Bowers arthroplasty for malunited fractures of the distal end of the radius. *J Bone Joint Surg Am*. 1988;70(10):1538–1551.
13. Jupiter JB, Ring D. A comparison of early and late reconstruction of malunited fractures of the distal end of the radius. *J Bone Joint Surg Am*. 1996;78(5):739–748.
14. Cooney WP III, Dobyns JH, Linscheid RL. Complications of Colles' fractures. *J Bone Joint Surg Am*. 1980;62(4):613–619.
15. Gartland JJ Jr, Werley CW. Evaluation of healed Colles' fractures. *J Bone Joint Surg Am*. 1951;33(4):895–907.
16. Gliatis JD, Plessas SJ, Davis TR. Outcome of distal radial fractures in young adults. *J Hand Surg Br*. 2000;25(6):535–543.
17. Geissler WB, Fernandez DL, Lamey DM. Distal radioulnar joint injuries associated with fractures of the distal radius. *Clin Orthop Relat Res*. 1996;327:135–146.
18. Athwal GS, Ellis RE, Small CF, Pichora DR. Computer-assisted distal radius osteotomy. *J Hand Surg Am*. 2003;28(6):951–958.
19. Murase T, Oka K, Moritomo H, Goto A, Yoshikawa H, Sugamoto K. Three-dimensional corrective osteotomy of malunited fractures of the upper extremity with use of a computer simulation system. *J Bone Joint Surg Am*. 2008;90(11):2375–2389.
20. Bronstein AJ, Trumble TE, Tencer AF. The effects of distal radius fracture malalignment on forearm rotation: a cadaveric study. *J Hand Surg Am*. 1997;22(2):258–262.
21. Crisco JJ, Moore DC, Marai GE, et al. Effects of distal radius malunion on distal radioulnar joint mechanics–an in vivo study. *J Orthop Res*. 2007;25(4):547–555.
22. Kihara H, Palmer AK, Werner FW, Short WH, Fortino MD. The effect of dorsally angulated distal radius fractures on distal radioulnar joint congruency and forearm rotation. *J Hand Surg Am*. 1996;21(1):40–47.
23. Hirahara H, Neale PG, Lin YT, Cooney WP, An KN. Kinematic and torque-related effects of dorsally angulated distal radius fractures and the distal radial ulnar joint. *J Hand Surg Am*. 2003;28(4):614–621.
24. Gordon KD, Kedgley AE, Ferreira LM, King GJ, Johnson JA. Design and implementation of an instrumented ulnar head prosthesis to measure loads in vitro. *J Biomech*. 2006;39(7):1335–1341.
25. Fraser GS, Ferreira LM, Johnson JA, King GJ. The effect of multiplanar distal radius fractures on forearm rotation: in vitro biomechanical study. *J Hand Surg Am*. 2009;34(5):838–848.
26. Berme N, Cappozzo A, eds. Biomechanics of Human Movement: Applications in Rehabilitation, Sports and Ergonomics. Worthington, OH: Bertec Corp.; 1990.
27. Dunning CE, Duck TR, King GJ, Johnson JA. Simulated active control produces repeatable motion pathways of the elbow in an in vitro testing system. *J Biomech*. 2001;34(8):1039–1048.
28. Gordon KD, Roth SE, Dunning CE, Johnson JA, King GJ. An anthropometric study of the distal ulna: implications for implant design. *J Hand Surg Am*. 2002;27(1):57–60.
29. Gordon KD, Dunning CE, Johnson JA, King GJ. Influence of the pronator quadratus and supinator muscle load on DRUJ stability. *J Hand Surg Am*. 2003;28(6):943–950.
30. Bowers WH. Instability of the distal radioulnar articulation. *Hand Clin*. 1991;7(2):311–327.
31. Lawler E, Adams BD. Reconstruction for DRUJ instability. *Hand (N Y)*. 2007;2(3):123–126.
32. Shaaban H, Giakas G, Bolton M, Williams R, Scheker LR, Lees VC. The distal radioulnar joint as a load-bearing mechanism–a biomechanical study. *J Hand Surg Am*. 2004;29(1):85–95.
33. Markolf KL, Lamey D, Yang S, Meals R, Hotchkiss R. Radioulnar load-sharing in the forearm. A study in cadavera. *J Bone Joint Surg Am*. 1998;80(6):879–988.
34. Markolf KL, Dunbar AM, Hannani K. Mechanisms of load transfer in the cadaver forearm: role of the interosseous membrane. *J Hand Surg Am*. 2000;25(4):674–682.
35. Shepard MF, Markolf KL, Dunbar AM. Effects of radial head excision and distal radial shortening on load-sharing in cadaver forearms. *J Bone Joint Surg Am*. 2001;83(1):92–100.
36. Shepard MF, Markolf KL, Dunbar AM. The effects of partial and total interosseous membrane transection on load sharing in the cadaver forearm. *J Orthop Res*. 2001;19(2):587–592.
37. Nishiwaki M, Nakamura T, Nagura T, Toyama Y, Ikegami H. Ulnar-shortening effect on distal radioulnar joint pressure: a biomechanical study. *J Hand Surg Am*. 2008;33(2):198–205.